Featured in Physics

Compressed ultrafast photography of plasmas formed from laser breakdown of dense gases reveals that internal processes dominate evolution at early times

Peng Wang,[1] Yogeshwar Nath Mishra,[1,2,*] Seth Pree,[3] Lihong V. Wang,[1,†] Dag Hanstorp,[4] John P. Koulakis,[5] Daniels Krimans,[5] and Seth Putterman[5,‡]

[1]*Caltech Optical Imaging Laboratory, Andrew and Peggy Cherng Department of Medical Engineering and Department of Electrical Engineering, California Institute of Technology, 1200 East California Boulevard, Mail Code 138-78, Pasadena, California 91125, USA*

[2]*Science Division, Jet Propulsion Laboratory, California Institute of Technology, 4800 Oak Grove Drive, Pasadena, California 91109, USA*

[3]*Department of Applied Physics, California Institute of Technology, 1200 East California Boulevard, Mail Code 128-95, Pasadena, California 91125, USA*

[4]*Department of Physics, University of Gotenburg, SE 412 96 Gothenburg, Sweden*

[5]*Department of Physics and Astronomy, University of California, Los Angeles, Los Angeles, California, USA*

(Received 27 July 2025; accepted 4 December 2025; published 30 January 2026)

Compressed ultrafast photography (CUP) is applied to laser breakdown in argon and xenon under pressures up to 40 bars to obtain two-dimensional images of the plasma dynamics of single events with a spatial resolution of 250 × 100 pixels and an equivalent frame rate of 500 GHz. Light emission as a function of position and time is measured through red, green, blue, and broadband filters. The spatially encoded and temporally sheared image normally used in CUP is now enhanced by the introduction of a constraint given by a spatially integrated and temporally sheared unencoded signal. The data yield insights into the temperature, opacity, the plasma formation process, and heat flow within the plasma and to the surrounding ambient gas. Contours of constant emission indicate that plasmas formed from sufficiently dense gas contract rather than expand despite having a temperature of a few eV. Plasmas formed from relatively low pressure gases such as 7-bar argon can radiate with emissivity near unity. Modeling transport and opacity as arising from inverse Bremsstrahlung requires a degree of ionization that strongly exceeds expectations based on Saha's equation even as customarily modified to include density and screening. According to this model, both electrons and ions are strongly coupled with a plasma coefficient $\gtrsim 1$. During the first few nanoseconds after formation, Stefan-Boltzmann radiation and thermal conduction to ambient gas are too weak to explain the observed cooling rates, suggesting that transport within the plasma dominates its evolution. Yet, thermal conduction within the plasma itself is also small as indicated by the persistence of thermal inhomogeneities for far longer timescales. The fact that plasma is isolated from the surroundings makes it an excellent system for the study of the equation of state and hydrodynamics of such dense plasmas via the systems and techniques described.

DOI: 10.1103/3vw9-h2g5

I. INTRODUCTION

In a strongly coupled plasma (SCP) the electrostatic potential energy is comparable to or greater than the thermal kinetic energy so that the fundamental plasma parameter $\Gamma = e^2/akT \gtrsim 1$, where e is the fundamental unit of charge, T is the temperature, $ax^{1/3} = a_0 = (3/4\pi n_0)^{1/3}$, n_0 is the atomic density and $x \leqslant 1$ is the degree of ionization. This regime is important for the study of astrophysical objects (e.g., white dwarf stars [1,2]), dusty plasmas [3], ultracold atom and ion trapping [4,5], ultrafast laser breakdown [6,7], photoelectron sources [8] and inertial confinement fusion [9]. It should be contrasted with, say, Tokamak plasmas where the density is low and the temperature is high so that $\Gamma \ll 1$ and where the constituent particles are weakly interacting, similar to those in an ideal gas. On the other hand, for example, warm dense matter is a strongly coupled plasma which is described by Saumon *et al.* [10] as a regime where "all the physics is important." Despite numerous studies, controlling and measuring strongly coupled plasmas is a challenge that is here addressed with the application of Compressed Ultrafast Photography (CUP) [11,12] to the laser breakdown of a dense gas which we believe shows strong coupling. Data generated by this technique show that on the nanosecond timescale the breakdown plasma is only weakly coupled to the environment so that its intrinsic thermohydrodynamic properties can be probed.

Due to the long-range nature of the Coulomb forces and the resulting correlation between particles, the macroscopic response of a SCP is also expected to be long ranged [13–16] as compared to Navier-Stokes hydrodynamics. So a line of attack for investigating SCP is to image its macroscopic motions. This is achieved by using CUP to capture the time-resolved, two-dimensional evolution of a SCP that is created by laser breakdown of dense argon and xenon. Example data that can be obtained with this technique are shown in Figs. 1–4. Figure 1 shows the evolution of a plasma formed from laser

*Present Address: Department of Physics, Indian Institute of Technology Jodhpur, Rajasthan 342030, India.

†Contact author: LVW@caltech.edu

‡Contact author: puherman@ritva.physics.ucla.edu

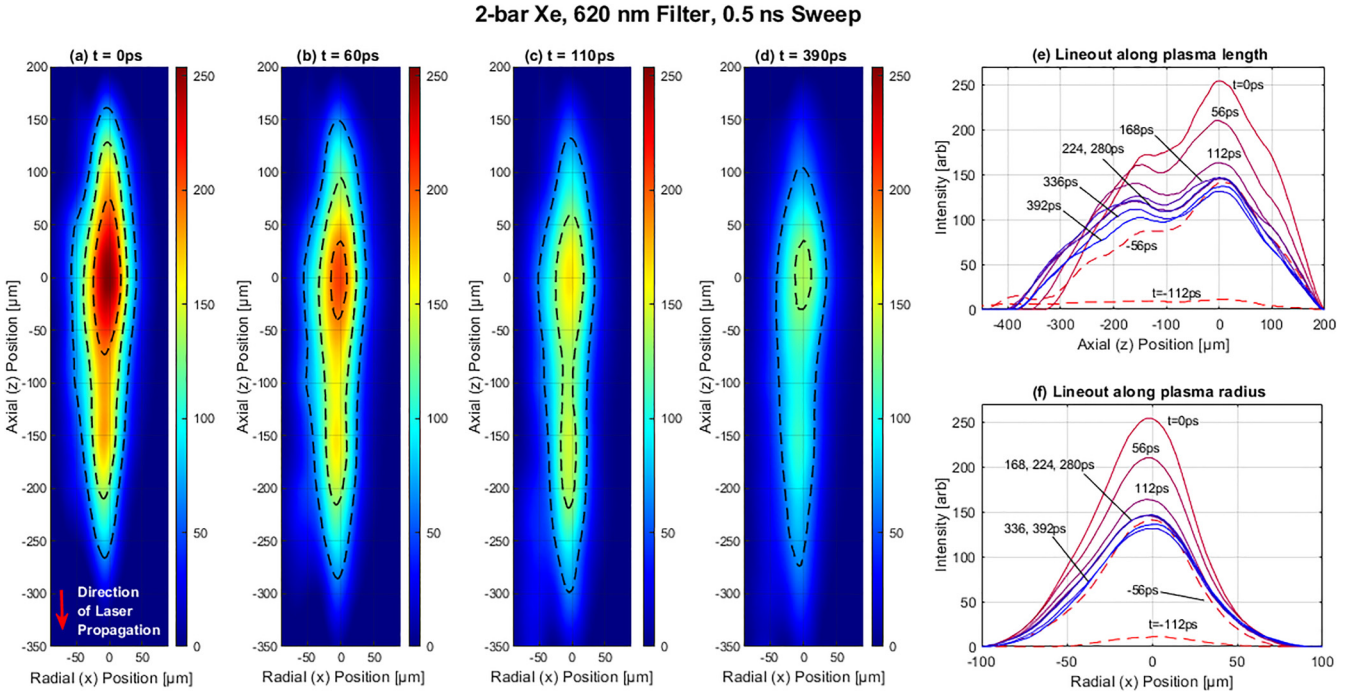

FIG. 1. [(a)–(d)] Four frames of the breakdown of 2-bar xenon with a CUP sweep setting of 0.5 ns. Extracted frames are at $t = 0$ (peak emission), 60, 110, and 390 ps. A single-shot movie has 400 frames. The intensity is false colored and in arbitrary units. Topographic lines of constant intensity are at 25%, 50%, and 75% of the peak intensity of each frame. [(e), (f)] Lineouts of the axial z and radial x dependence of the emission during the first 400 ps. The lines cross the region of maximum emission intensity. These data are from a single event. The fact that CUP has accurately captured multiple peaks in the axial direction is confirmed by traditional streak photos (see the Supplemental Material, Fig. S7 [17]).

breakdown of 2-bar xenon as measured through a filter centered on 620 nm. Breakdown is driven by a focused 0.9-mJ, 220-fs-long pulse of 800 nm light using a windowed pressure cell [7]. Figure 2 shows the intensity of emission from the bright central region of breakdown of 7-bar argon as taken through 620-nm ("Red"), 515-nm ("Green"), and 415-nm ("Blue") filters. The plotted emission intensity per steradian has been scaled to $\bar{I}_\lambda = I_\lambda \lambda^5/2hc^2$. Figure 3 shows the rise of the plasma emission for different positions along the plasma length. Since the curves at various positions have the same shape, we interpret the measured rise time as being limited by the system's temporal resolution. Nonetheless, the time delay between curves at different positions gives information about the plasma formation processes. Figure 4 shows the evolution of contours of constant emission that are normalized to the instantaneous peak intensity for 7- and 25-bar argon. These frames and intensity curves come from single-shot data acquisitions and are not the result of patching together separate pump and probe acquisitions. The equivalent frame rate can reach 500×10^9 frames per second (fps), though we estimate the resolution to be 30 ps.

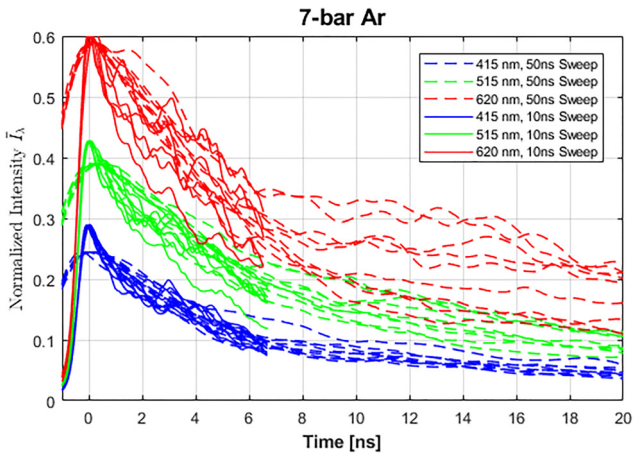

FIG. 2. The measured emission (units of $\mathrm{MW\,m^{-2}\,nm^{-1}}$ per steradian) from the brightest 5×5 pixel region has been scaled with $\lambda^5/2hc^2$ to yield a dimensionless emission. Each trace is a single shot through Red (620 nm), Green (515 nm), and Blue (415 nm) filters for 10-ns and 50-ns sweeps.

Analysis of the spectral components indicates that argon and xenon at pressures above 7 bars emit with emissivity close to unity and are opaque. At these atomic densities, the experimentally measured opacity requires a degree of ionization $x \gtrsim 1$ assuming that opacity arises from inverse Bremsstrahlung. Combined with our measurement of temperature, we find that Γ is of order unity for both electrons and ions. These systems can therefore be characterized as strongly coupled plasmas.

The goal of this communication is to describe the experiment which acquires the above data and the theoretical analysis which leads us to conclude the following:

(1) Stefan-Boltzmann radiation from the argon plasma is small compared to the measured changes in the energy of the plasma.

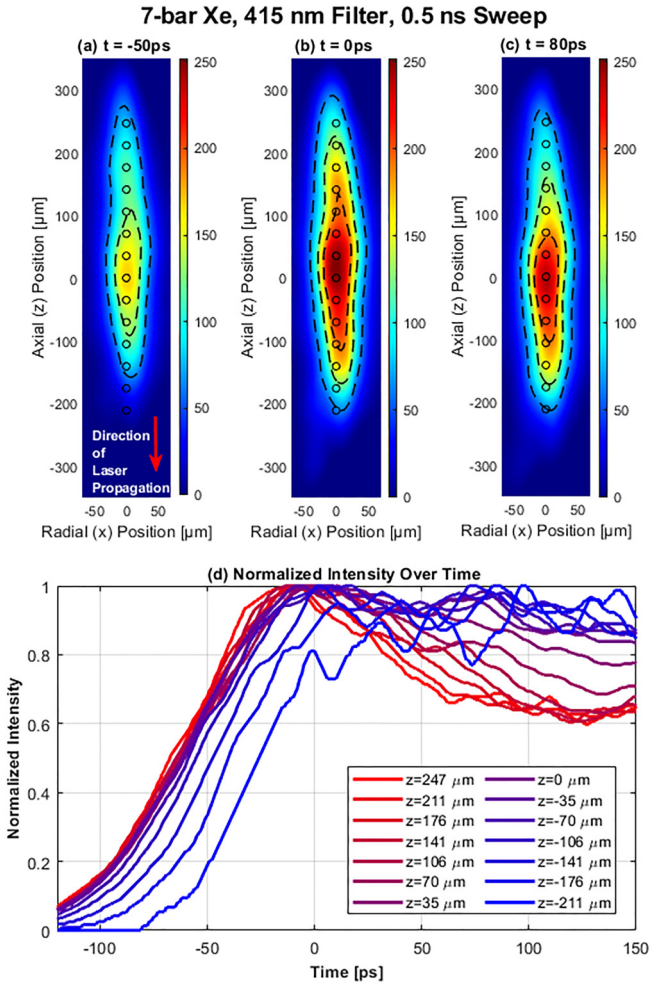

FIG. 3. Rise of plasma emission as a function of position. Frames at (a) $t = -50$ ps, (b) $t = 0$ ps, and (c) $t = 80$ ps, respectively, where $t = 0$ is the time of peak emission. Circles in the frames indicate the positions where the light emission is plotted over time in panel (d). Emission in (d) is normalized by the peak of each curve.

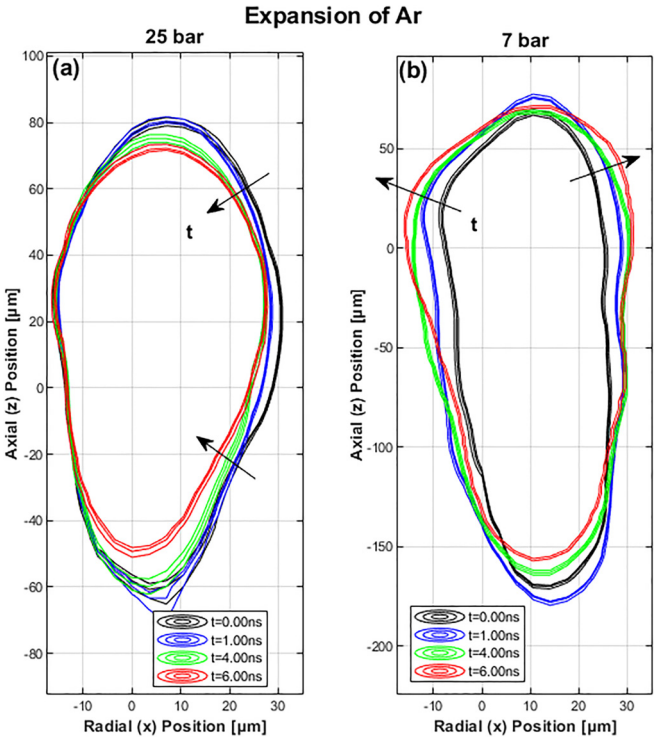

FIG. 4. Expansion of the breakdown plasma resolved by single-shot CUP. The evolution of (a) 25-bar argon and (b) 7-bar argon. Contours are drawn at $50 \pm 1\%$ of the maximum intensity at various times. The relative position of the contours indicates the expansion of the plasma. For plasmas formed at high density, the contours steepen and the plasma contracts, whereas at 7 bars the plasma expands.

(2) Thermal conduction of energy to the surrounding ambient gas at 300 K is also small compared to the observed changes in energy.

It follows that the response is dominated by the internal thermohydrodynamics of a strongly coupled plasma. Initially the plasma is not uniform and has a hot center and colder edges. As time evolves, the plasma cools, but rather than spatially evening out, with hot spots getting cooler and cold spots warmer, the emission drops locally in a way that its profile, including initial inhomogeneities, maintains its shape. This persistence of inhomogeneities within the plasma implies the following:

(3) The electron thermal conductivity inside the plasma is small compared to the timescale of the other transport processes.

(4) Local processes dominate thermal equilibration between species. If τ_{e-th} is the timescale over which the temperature of electrons and ions equilibrate, we arrive at the same conclusion as Bataller, *et al.* [7] and interpret the rapid drop in emission at early times $t < \tau_{e-th} \lesssim 1$ ns for the higher pressures as arising from electron-ion equilibration [7,18].

As the plasma cools and the electrons and ions equilibrate, some electrons will recombine and impart their ionization energy back to the electron gas causing recombination heating [19,20]. But,

(5) Signatures of recombination heating are not observed.

We speculate as to whether the effects of screening [21,22] are much greater than is theoretically proposed [23,24] for the parameter space realized in these experiments.

Certain regimes of SCP are predicted to have a tensile strength (negative pressure) [25]. Laser breakdown in lower-pressure (lower-density) gas immediately expands radially, consistent with ideal gas dynamics and positive pressure plasma. At higher pressure,

(6) The plasmas display a lack of expansion, if not contraction, indicative of strong nonideal interactions.

This suggests that these systems might be a route to investigating the hydrodynamic consequences of the tensile strength of SCPs.

II. EXPERIMENT

The experiment (Fig. 5) uses a customized high-pressure chamber system built by Bataller, *et al.* [6,7] which supplies high-purity noble gas with adjustable and accurate pressure. A Ti:Sapphire femtosecond laser (Coherent) centered at 800 nm passes through a 60-mm focal length lens to induce

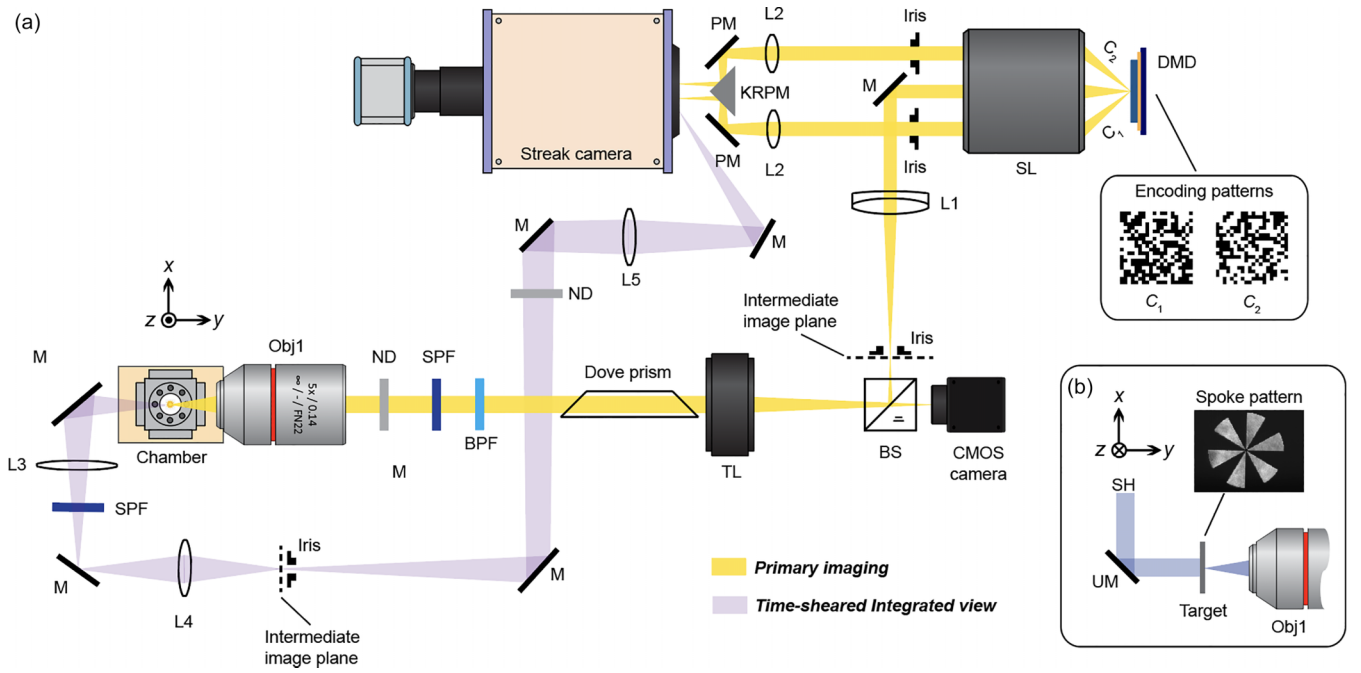

FIG. 5. Experimental CUP setup. (a) Laser pulse propagating in the z direction causes breakdown in the chamber. The yellow path provides spatially dependent emission to the CMOS camera and streak camera. Prior to time shearing by the streak camera, the signal passes through a coded aperture provided by a DMD. The intermediate image plane, DMD, and streak camera photocathode are conjugate planes. The purple path provides spatially integrated emission to the streak camera, which is a key constraint to the image reconstruction process introduced in this work. (b) The second harmonic of the femtosecond laser is used to illuminate a test target for the purpose of measuring the response of the coded aperture acquisition and CUP inversion to a delta function, which forms the basis for selection of the optimal mask (see Supplemental Material Sec. 1.11 [17]). Various optical elements such as bandpass filters (BPFs) and prisms (PMs) are employed and listed with labels in Supplemental Material Table S1.

breakdown at the center of the gas chamber, where it arrives with an energy of 0.9 mJ. The laser beam propagates in the z direction, is linearly polarized in the x direction (see Fig. 5), and has a pulse duration tunable from 60 fs up to a few picoseconds. In this work, a temporally chirped pulse with 220 fs duration was optimized and chosen to generate a plasma with brightest emission (Supplemental Material Fig. S9 [17]). See the full characterization of the laser system in the Supplemental Material, Figs. S5 and S6 [17]. The imaging system observes the plasma through a high-transmission quartz window on one side of the chamber. An infinity-corrected objective lens in conjunction with a tube lens forms an intermediate image, which is split into two copies by a beam splitter: one is recorded by a conventional complementary metal oxide semiconductor (CMOS) camera (static view) and the other is further processed to form the time-sheared dynamic view. In this latter beam path, a digital micromirror device (DMD) (Texas Instruments) encodes the image by displaying a computer-generated two-dimensional (2D) static pseudorandom binary pattern. Thanks to the modulation mechanism of tilting mirrors, two complementary encoded images are reflected by the DMD in two separate directions. They are subsequently relayed and rerouted to a streak camera (Hamamatsu) side by side without overlap. Inside the streak camera, temporal shearing of the frames in the dynamic scene achieves from 1×10^6 to 1×10^{12} fps. Signal synchronization between the laser and the streak camera is critical for the acquisition of any transient event. Eventually, one single femtosecond-laser pulse generates one single spatially encoded temporally sheared raw image of one complete evolution of 2D plasma dynamics on the streak camera. Images are 250×100 pixels, and each pixel corresponds to a 3.5×3.5 μm^2 plasma area. See the Supplemental Material for experimental setup and components [17].

Emission spectra are measured through narrow-band filters centered at 410, 515, and 620 nm, and a broadband filter covering the entire visible light spectrum (350–650 nm). The first three are extensively exploited to characterize the temperature and emissivity properties of blackbody radiation from plasma.

Important to the interpretation of the data is an auxiliary view (purple path) introduced here, which is taken from another window and projected directly to an unused region on the streak camera. It is spatially integrated and time sheared and provides a key constraint on image reconstruction. In addition, a small portion of the original laser pulse is frequency doubled to a 400-nm second harmonic (SH) pulse by a nonlinear beta barium borate (BBO) crystal. This SH pulse flood illuminates the chamber through its back window, which is essential in imaging and temperature calibration and is described in Supplemental Material Sec. 1.4 [17].

Recovering and decompressing the three-dimensional (3D) spatiotemporal (x, z, t) dynamics of the observed event from the two simultaneously acquired 2D images, one from the CMOS camera and one from the streak camera, is a typical ill-conditioned inverse problem due to multiplexing and

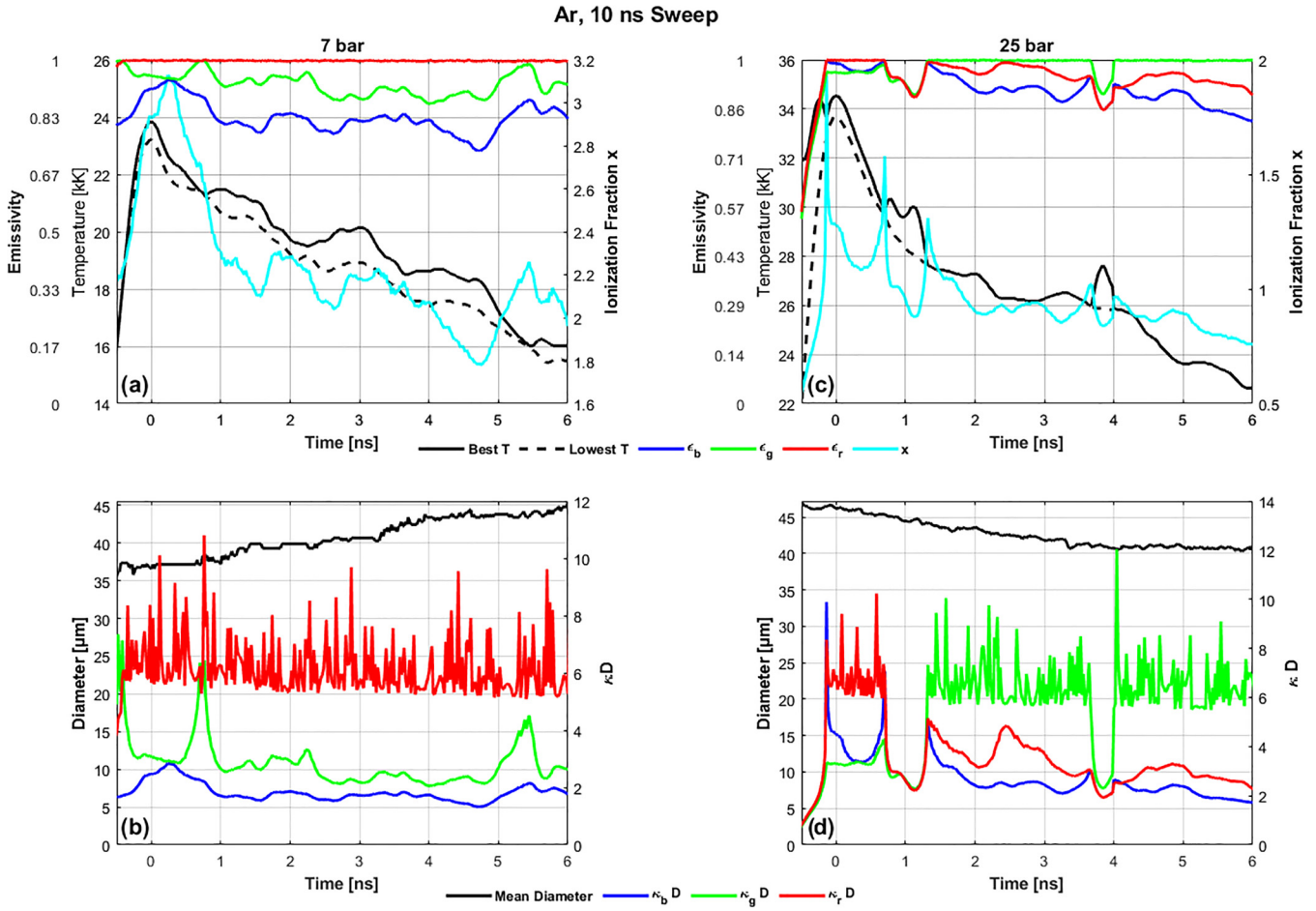

FIG. 6. Temperature, emissivity, ionization, mean diameter D, and optical thickness (κD) for breakdown in [(a), (b)] 7-bar and [(c), (d)] 25-bar argon for 10-ns sweep. Temperature is based upon emission from the central region of the plasma. Emissivities ϵ_r, ϵ_g, and ϵ_b are displayed for the best-fit temperature. The dashed line is the minimum temperature at which the separate emissivities are all $\leqslant 1$. The degree of ionization is determined from the lowest emissivity, which is generally the blue curve. The singularity in transport properties which accompanies emissivities close to unity leads to the spikes that can be seen in the curves for κD, which is the photon mean free path.

high compression, the solution of which can only be reached by resorting to regularization [12]. Different from previous CUP modalities, the additional viewing channel introduced transforms the 3D data cube to a time sequence by 2D spatial integration. This added perspective toward the 3D domain presents a new angle of projection based on the theory of Radon transformation, potentially enforcing higher fidelity in reconstruction [12] and thus featuring a technological advancement from this work. The image-forming pipeline, which is based on the assumption of data sparsity in the gradient domain, is discussed in Supplemental Material Sec. 2.2 [17], which includes references [26–29].

III. ANALYSIS

Temperature and emissivity ϵ are determined by fitting the emission of the brightest 7×7 pixel region of the plasma in the three listed windows. In general, the measured emission is $\bar{I}_\lambda = \epsilon_\lambda / [\exp(hc/\lambda kT) - 1]$, where the emissivity ϵ_λ is unity for a Planck blackbody but in general depends on wavelength. One restriction on T is that $\epsilon_\lambda \leqslant 1$. In other words, there is a minimum T at which one of the colors has $\epsilon = 1$ with the other wavelength having $\epsilon_\lambda < 1$. This value of T is plotted in Fig. 6 as a lower bound. Motivated by the graybody approximation, where ϵ_λ is independent of wavelength, we choose a higher temperature which minimizes the spread in ϵ_λ. This temperature, along with the various ϵ_λ values, is also plotted in Fig. 6. The fact that ϵ_λ is close to unity for the three wavelengths analyzed implies that the plasma is nearly opaque and the blackbody emission model is reasonable.

A key parameter is the degree of ionization, x. It determines the kinetic and ionization energy of a gas consisting of ions, free electrons, and neutral atoms:

$$E = \tfrac{3}{2} n_0 k (T_i + xT) + n_0 x \chi_0, \tag{1}$$

where n_0 is the number of atoms in the plasma, T_i is the ion or neutral temperature, χ_0 is the tabulated ionization energy, and we have allowed for the possibility that the electron temperature T has not yet equilibrated with the ions and/or neutrals. To obtain x from the spectral data requires a higher level of theory as it involves an analysis of opacity and emissivity. We start with the Nekrasov formula [30], which connects the emissivity of an infinite cylinder with diameter D

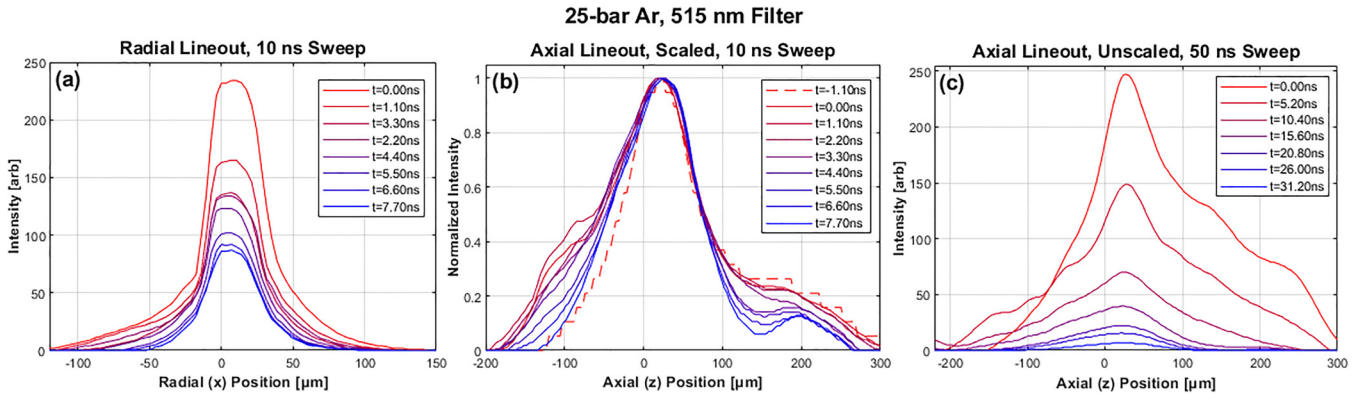

FIG. 7. Emission of a single shot along a lineout crossing the brightest pixels for 25-bar argon acquired through a 515 nm filter: (a) radial lineout for a 10-ns sweep, (b) axial lineout for a 10-ns sweep that is scaled to the peak value, and (c) axial lineout for a 50-ns sweep. The rapid drop in emission in (a) during the first nanosecond is due to local equilibration of electrons, ions, and neutrals. Notice that the central peak in (b) maintains its curvature for at least 10 ns, which indicates the low level of thermal conduction within the plasma.

(estimated as the full-width-at-half-maximum emission) to the attenuation of light of wavelength λ (κ_λ) in the plasma, $\epsilon_\lambda = 1 - \exp(-\kappa_\lambda D)$. This is an approximation as our aspect ratio is about 4. In view of the featureless spectra observed here and in previous experiments [7,31], we interpret the attenuation κ in terms of inverse Bremsstrahlung, which is free-free scattering of electrons. The free electrons are accelerated by the electric field in the presence of a linear damping that is due to a frequency-dependent electron collision time τ_ω [31,32]. In this Drude model [32], the imaginary part of the wave vector in the resulting dispersion law is interpreted as the attenuation κ_λ and we work in the parameter region where the frequency of light $\omega = 2\pi c/\lambda > \omega_p$, where ω_p is the plasma frequency. Following the perspective of Ref. [33], we incorporate strongly coupled behavior into this binary collision theory with a collision time that is modified to include the effects of strong coupling [18,31,32] and the molecular dynamics simulations of Ref. [18] in the limit $\bar{\omega} = \hbar\omega/kT \ll 1$. As the resulting degree of ionization generally leads to a plasma coefficient $\Gamma \sim 1$, we neglect electron neutral scattering and account for strong coupling with the collision time consistent with Ref. [18] and find

$$\kappa_\omega = \frac{k_0\gamma}{\omega\tau_\omega} = x^n A \ln\Lambda, \quad \gamma = \frac{\omega_p^2}{\omega^2} = \frac{4\pi n_0 x e^2}{m\omega^2}, \tag{2}$$

$$f(\bar{\omega}) = \frac{1-\exp(-\bar{\omega})}{\bar{\omega}}, \quad \Lambda = 1 + \frac{B}{x^{n-3/2}}, \tag{3}$$

$$A = \frac{2}{\sqrt{6\pi}}\frac{\omega}{c}\frac{\omega_{p,1}^3}{\omega^3}\Gamma_1^{3/2} f(\bar{\omega}), \quad B = \frac{0.7}{\sqrt{3}f(\bar{\omega})^{3/2}\Gamma_1^{3/2}}, \tag{4}$$

where m and Γ are the mass and plasma coupling constant of an electron and k_0 is the vacuum wave number. The subscript 1 means "evaluated at $x = 1$"; for $x < 1$, $n = 2$, and for $x > 1$, $n = 3$. When $x > 1$, the level of ionization, Z, of some of the ions is also greater than unity. In this case, we have approximated $\langle Z\rangle = x$ and used $\Gamma = xe^2/a_0kT$, which matches τ_ω in Ref. [7]. In the limit $\bar{\omega} \ll 1$ the collision time obtained by inverting Eq. (2) matches the strong-coupling collision time simulated with molecular dynamics in Ref. [18] with Λ given by Eq. (3). When $\bar{\omega} > 1$ the induced emission described by $f(\bar{\omega})$ leads to the well-known Bremsstrahlung attenuation formula [34] provided that now $\ln\Lambda$ is of order unity. While we have provided a qualitative formula that is physically useful for interpreting experiments, the accuracy of using Drude as an intermediate model needs to be evaluated. One possibility is the molecular dynamics calculations of Ref. [35] when extended to include attenuation. Note that our formulas can be applied to arbitrary x.

Emission and degree of ionization are determined by the electron temperature T. To obtain x via opacity also requires the plasma diameter D, which is supplied by the radial lineout of intensity of emission as displayed for a single shot in Fig. 7(a). Values of D and also x are displayed in Fig. 6 as well.

IV. BLACKBODY RADIATION IS SMALL

Blackbody radiation per unit surface area of the plasma [36] is σT^4, where σ is the Stefan-Boltzmann constant. In the approximation that the plasma is a cylinder with diameter D and length L, the loss in energy due to radiation is $dE/dt|_r = -\pi DL\sigma T^4$. The plasma energy will have contributions from the kinetic energy of ions, electrons, and neutrals, as well as the potential energy of ionization. We first consider 25-bar argon at times after 2 ns so as to exclude the initial rapid drop in emission which is ascribed to electron-ion thermal equilibration. Then the kinetic energy per unit volume is $(3/2)n_0(1+x)kT$, where n_0 is the density of the ambient, 300-K, 25-bar gas. Cooling due to blackbody radiation is $dT/dt|_r = -8\sigma T^4/[3kDn_0(1+x)]$. Using $n_0 = 6.2\times10^{20}$ cm^{-3} and $D = 43$ μm yields cooling at a rate of 110 K ns^{-1} for parameters of $x = 0.9$ and $T = 27$ kK that apply at 2 ns. A fit to the temperature in Fig. 6 gives

$$T(t) = T(0) + A[e^{-t/\tau} - 1] - Bt, \tag{5}$$

where $T(0) = 3.05$ eV, $A = 0.5$ eV, $B = 0.1$ eV ns^{-1}, and $\tau = 0.33$ ns so that the observed cooling rate is $B \simeq 1100$ K ns^{-1}. The tenfold higher cooling rate observed implies that radiative cooling is small and that other processes are more important. Inclusion of the ionization potential would increase the heat capacity and further decrease the magnitude of the calculated cooling, should x be a decreasing function

of T. This conclusion is not sensitive to the assumptions underlying Eqs. (2)–(4).

V. CONDUCTION TO AMBIENT GAS

Thermal conduction to the exterior ambient gas is limited by the thermal conductivity of the surrounding ambient argon, which is neutral. The maximum heat flow is realized under the assumption that the plasma temperature is constant with a step function initially at the boundary. This would happen in the limit where thermal conductivity in the plasma is much larger than in the surrounding ambient gas. This upper bound to cooling of the plasma with diameter D is [37]

$$\frac{\Delta T}{T} = -\frac{5}{6(x+1)}\sqrt{\frac{\chi_T t}{\pi D^2}}, \tag{6}$$

where $\chi_T \approx 6\times10^{-4}$ μm^2 ns^{-1} is the tabulated thermal diffusivity of the ambient, neutral argon which surrounds the plasma and limits the heat flow to the environment. We are using the same plasma model as for the discussion of radiative cooling. For $t = 4$ ns and $x = 0.6$ this yields $\Delta T/T = 3\times10^{-4}$, which is again small compared to the observed response of the plasma and not sensitive to the assumptions underlying Eqs. (2)–(4).

VI. TRANSPORT WITHIN THE PLASMA

The breakdown plasma in a real experiment will be characterized by a wide range of parameters. Assessment of the *a priori* unknown state of the plasma requires an interpretation of the transport timescales. Toward this goal, we consider four cases for the collision cross section σ:

(1) $\sigma_{e,\text{dilute}} \approx A r_T^2 \ln\Lambda$ is the long-established cross section for an electron-electron or electron-ion collision in a low Γ or hot plasma [38], where $r_T = \frac{Ze^2}{kT}$ is the impact parameter within which the collision is thermodynamically meaningful and $\Lambda = \delta_D/r_T$, where $\delta_D = \sqrt{kT/8\pi x n_0 e^2}$ is the Debye screening length. Following Dimonte and Daligault [18] and Stanton and Murillo [39], $A = 8\sqrt{2\pi}/3$. As an example, at 30 000 K, $r_T = 0.53$ nm (we take $Z = 1$ unless otherwise stated) and for a 7-bar gas $\delta_D = 0.66/\sqrt{x}$ nm, so that the dilute limit requires $x \lesssim 1/4$.

(2) $\sigma_{e,D} \approx \frac{32\sqrt{2\pi}}{3}\delta_D^2 = \frac{32\sqrt{2\pi}}{3}\frac{r_T^2}{6\Gamma^3}$ is the strong screening limit $\delta_D < r_T$ and applies when Γ is large. This expression is consistent with the insights of Kurilenkov and Valuev [40], who note that, when the Debye screening length becomes smaller than the impact parameter r_T, the screening length will determine the cross section. The expression will be used in the context of electron-electron transport processes. A numerical factor of 4 has been introduced so as to achieve a good fit with the unifying transport formula of Stanton and Murillo [39].

(3) $\sigma_{e\text{-int}} = \frac{8\sqrt{2\pi}}{3} r_T^2 \ln(1+\frac{b_0}{\sqrt{x}})$ applies to the intermediate values of $1 \lesssim \Gamma < 3$ and b is evaluated at $\bar{\omega} = 0$. This expression for cross section is a fit to precise molecular dynamic simulations in Ref. [18].

(4) $\sigma_{e\text{-}0} = 10^{-16}$ cm at 1 eV is the cross section for the collision of electrons with neutral argon atoms as measured by time of flight [41]. The corresponding collision time $\tau_{e\text{-}0} = 1/\mathrm{v_{th}} n_0 \sigma_{e\text{-}0}$ where $\mathrm{v_{th}} = \sqrt{kT/m}$ and m is the electron mass. This expression is applied when ionization is low.

VII. THERMAL CONDUCTION WITHIN PLASMA

Aside from conduction to the ambient gas, one can ask how heat moves to different locations within the plasma. In particular, how does thermal conduction within the plasma affect heat flow along the direction z of the laser pulse where maximum inhomogeneity is expected? Figure 7 shows lineouts through the region of peak emission at $r = 0$ and $z = 0$. Figure 7(a) displays an approximately threefold drop in emission during the first 10 ns. Despite this, as shown in Fig. 7(b), the curvature of the scaled emission profile barely changes with time, so that even within the plasma, thermal transport has a small effect on the emission profile on the resolved timescales. Although electrons are efficient transporters of heat [42], this observation is consistent with theory.

A general expression for the electron thermal diffusivity is $\chi_{T\text{-}e} = \frac{2\mathrm{v_{th}}}{3\sqrt{\pi}\sigma n}$ [42], where n is the density of scattering sites. This expression can be generalized to strong coupling via the choice of σ. The strongest thermal conduction is achieved for the smallest cross section, which is the limit where case 2 applies. As an estimate for this case, take $x \approx 1$ and $T = 30$ kK, $n_0 = 6.2\times10^{20}$ cm^{-3}, $\mathrm{v_{th}} = 6.9\times10^7$ cm s^{-1}, and $r_T = 5.3\times10^{-8}$ cm so that $\Gamma \gtrsim 0.7$, $\sigma = 2.5\times10^{-14}$ cm, to get $\chi_{T\text{-}e} = 0.17$ μm^2 ns^{-1}. The mean free path is $\ell \sim 1/n\sigma \sim 6.5\times10^{-8}$ cm. Consider the diffusive spread in time of a Gaussian fit to the data. The width $w(t)$ at 80% of the maximum should expand as $w^2(t) = w^2(0) + 3.6\chi_{T\text{-}e}t$. Using $w(0) \approx 60$ μm yields an increase in width less than 1 μm after 10 ns. This is consistent with experimental measurements which show that there is a very slight change in width, if not a contraction, during the first 7 ns. We return to this issue in Sec. XI below.

VIII. ELECTRON-ION EQUIPARTITION OF ENERGY

The laser directly excites the electrons on a femtosecond timescale and so creates a situation where the ions have an initial temperature $T_i < T$. The subsequent equilibration leads to a rapid drop in emission, which we interpret as a proxy for temperature, during the first nanosecond. As we have argued, there is insufficient heat flow to the ambient gas, and thermal conduction within the plasma is low as well. This leads one to interpret this drop as being due to electron-ion equipartition of energy. After equilibration the drop in emission is slower. This behavior is described with cross-section case 3, where collisions are partially screened [18,32], the parameter space for these experiments. When applied to electron-ion collisions the timescale for thermal equipartition will be increased by the ion/electron mass ratio to $\tau_{e\text{-th}} = (M/m)\tau_{e\text{-ion}}$, where $\tau_{e\text{-ion}} = 1/n_i\sigma_{e\text{-int}}\mathrm{v_{th}}$, M is the ion mass, and $n_i = xn_0$ is the density of ions (taking here $x < 1$). This early time equilibration is qualitatively apparent in Fig. 8 and the best fit to the temperature [Eq. (5)] yields a timescale of about 300 ps, which should be compared with the 200 ps estimated with cross-section case 3.

Ions can also be heated above their initial ambient temperature of ≈300 K by a process which is much faster than the collisional equilibration discussed above. In our

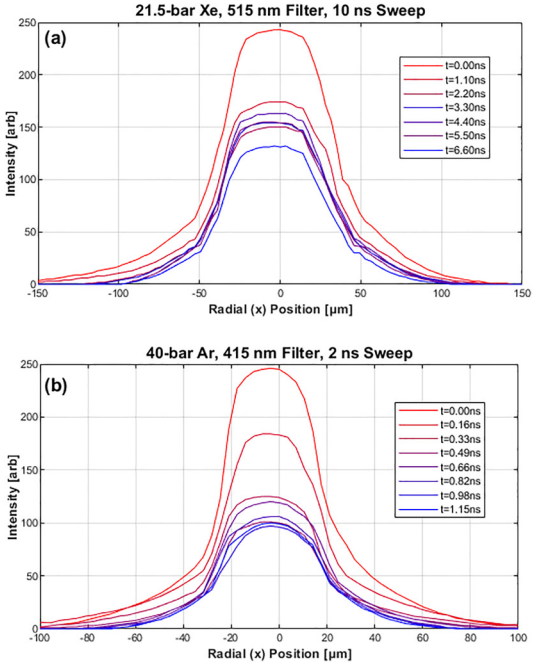

FIG. 8. Emission along a radial lineout through the brightest central pixels for (a) 21.5-bar xenon and (b) 40-bar argon. The rapid drop in emission during the first nanosecond is due to local equilibration of electrons with ions and neutrals.

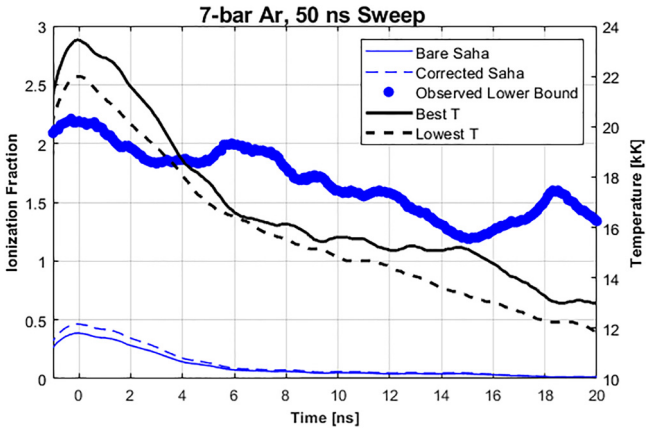

FIG. 9. Temperature and ionization level of 7-bar argon as compared to Saha's equation [Eq. (7)]. The thick blue line is the level of ionization as determined from emissivity and transport theory under the assumption that the photon mean free path is due to inverse Bremsstrahlung. The thin solid blue curve is the level of ionization calculated with Saha's equation and the dashed blue curve is calculated with the first-order screening effects included. Both calculations are well below the lower bound, which suggests a larger screening effect or some other large source of continuum lowering.

experiment, the laser pulse randomly rips electrons off the atoms on the femtosecond timescale. In this initial plasma state the ions have a two-particle correlation $g(r) = 1$. This function describes the probability of having two ions a distance r apart. However, $g(r) = 1$ does not match the values in thermodynamic equilibrium under the given plasma coupling parameter, $\Gamma_i = e^2/akT_i$ for $x < 1$ or $\Gamma_i = Z^2e^2/a_0kT_i$ for $Z \geqslant 1$, where Z is the degree of nuclear ionization. For the case at hand of 25-bar argon, $x = 0.73$ at $t = 0$, so $\Gamma_i \approx 65$. This high value of Γ_i means that the ions instantaneously constitute a very strongly coupled plasma which is out of the equilibrium determined by the nonlocal Coulomb forces. The approach to equilibrium results in a "disorder-induced heating" (DIH) [5,43], which occurs on a picosecond timescale which is much shorter than $\tau_{e\text{-th}}$. DIH would lessen the magnitude of the drop in emission that accompanies electron-ion equilibration; however, we are unable to separate the heating due to recombination from DIH. Nevertheless, this experimental arrangement should be an excellent platform for the study of DIH in a real plasma.

According to Fig. 7(b), emission decreases more rapidly for $z \approx 200$ μm with a decay rate that is approximately two to three times more rapid than at the peak. We interpret this rapid decay as being due to lower ionization with a corresponding increased contribution from the neutral atoms. In this situation, the effective cross section is described by case 4. This observation is made possible by the slow axial flow of heat.

IX. SCREENING AND LEVEL OF IONIZATION

Based upon emissivity which we interpret as arising from the scattering of light by free charges [7,21,42,44–46], the deduced degree of ionization, x, can be much larger than what follows from Saha's equation [21,22,44] even when leading-order screening effects [23,24] are included. Consider Fig. 9, which shows the breakdown emission response of 7-bar argon taken under the same physical conditions as Fig. 6, but for longer sweep or period of data acquisition. Since the ionization energy for argon is $\chi_0 = 15.76$ eV and the temperature is 2 eV or less, one would expect that the plasma is singly ionized at most. This supposition is confirmed by Saha's equation of ionization,

$$\frac{x^2}{1-x} = \frac{2g}{n_0\lambda_{\text{deB}}^3}e^{-\chi/kT}, \tag{7}$$

where the thermal de Broglie wavelength is $\lambda_{\text{deB}} = h/\sqrt{2\pi mkT}$, $n_0 = 1.7 \times 10^{20}$ cm^{-3}, $a_0 = 1.14$ nm, and for argon the degree of degeneracy is $g = 6$. According to Saha's equation, $x = 0.4$ at 2 eV ($t = 0$) and $x = .07$ at 1.4 eV, which is the temperature at 7.0 ns. The value of ionization deduced from opacity to blue light is much larger, being $x = 2.2$ ($t = 0$) and 2.0 ($t = 7$ ns). As blue emissivity is lowest, we have used that value for this calculation. The value of x calculated from red and green emissivities is regarded as a lower bound as these values are close to 1.

Saha's equation applies to an isolated atom and this version applies when only neutrals and singly ionized atoms are present so that doubly ionized atoms are inconsequential. In a dense gas the ionization potential is lowered by screening, which leads to an effective ionization potential [23,24],

$$\chi = \chi_0 - \frac{kT}{2}((1+\Lambda)^{2/3} - 1), \tag{8}$$

where $\Lambda = (3x^{1/3}\Gamma_1)^{3/2}$ (for $x < 1$). Calculations of the level of ionization based on the bare and supplemented Saha equations [Eqs. (7) and (8)] are plotted in solid and dashed blue curves in Fig. 9. Both lie well below the minimum level of

ionization observed and cannot account for the observed opacity based upon the attenuation of light being due to inverse Bremsstrahlung. Either opacity is due to different dynamics, or some new process [44] is contributing to a further lowering of the ionization energy.

X. LACK OF RECOMBINATION HEATING

Figures 6 and 9 show the cooling of a 7-bar argon plasma at a rate of 1100 K ns^{-1} between 0 and 5 ns. Let us compare this to the average cooling due to blackbody radiation at the intermediate temperature of 20 000 K at 2 ns, where $D =$ 40 μm. This would lead to a temperature drop of 90 K ns^{-1} when the heat capacity is that of an ideal gas. This difference is accentuated when the possibility of recombination heating is evaluated [47]. From Eq. (1), a change in the degree of ionization $\Delta x = x(0) - x_f$ also would not only inhibit cooling but lead to heating as implied by energy balance:

$$\frac{3}{2}(1+x_f)kT_f = \frac{3}{2}(1+x(0))kT_0 + \Delta x\chi_0 + \frac{1}{N_0}\int_0^f \left.\frac{dE}{dt}\right|_r dt, \tag{9}$$

where the subscripts f and 0 refer to the final and initial states. The last term is the radiated energy, and for the purpose of developing this argument, we are using the bare ionization potential. Figure 9 shows that the degree of ionization, as determined by opacity to blue light, decreases by $\Delta x = 0.6$ during the interval $0 < t < 10$ ns. Using $T(0\text{ ns}) = 23\,600$ K and $\Delta x = 0.6$ leads to $T_f = 2.4T(0)$ when $\chi_0 = 15.8$ eV. This is a very large heating and there is no such signature in the data. We propose that a larger-than-expected reduction in the ionization potential could account for both the high ionization and weak recombination heating.

There are other sources of cooling. An expanding plasma does work against the exterior gas. In view of the large pressure and temperature difference between the inside and outside of the plasma channel, this effect is small. The hydrodynamic kinetic energy developed in an expanding plasma has also not been included in the energy balance. Increases in this quantity during an expansion can lead to adiabatic cooling [48], which is discussed in the next section. When the region of emission expands, we propose a means whereby screening can lead to cooling. Emission from newly formed plasma requires local ionization, which comes at the expense of recombination further inside the plasma, where the ionization energy is lower due to screening.

XI. LACK OF EXPANSION

A possible source of cooling is the adiabatic expansion of a gas. Our experiment provides single-shot, time-resolved measurements of the plasma's two-dimensional macroscopic motion, enabling us to observe its changing shape over time as, for instance, indicated in Fig. 4. To what extent do these data give further insight into cooling and hydrodynamic motions?

In a simple model, laser breakdown creates an initial condition with a spatial discontinuity in pressure and temperature at constant mass density. According to the Euler equations, such a contact discontinuity generates an outgoing shock wave as well as an expanding entropy (temperature) wave. In an ideal gas in one dimension, such an entropy discontinuity initially propagates outward at the speed $u/2\gamma$, where $u(T, x)$ is the speed of sound on the hot side, and γ is the adiabatic index. The supplemental material shows this effect for the case where $T/T_0 = 100$ and $\gamma = 5/3$ (see Fig. S13 [17]).

The initial state of the breakdown plasma also includes a discontinuity in ionization. So the ideal gas kinetic pressure, $p = n_0(kT_i + xkT)$, is higher than used in the above model. For 25-bar argon after electrons and ions have equilibrated, $T \approx 28$ kK and $x \approx 1$, leading to $p \approx 4800$ bars. Using the adiabatic coefficient $\gamma = 5/3$, a characteristic sound velocity is $u \approx \sqrt{\gamma p/n_0 M_{\rm Ar}} \approx 4.4$ μm ns^{-1}. For 7-bar argon the characteristic temperature at 2 ns is 19 kK with $x \approx 2$, yielding $u \approx 4.4$ μm ns^{-1}.

Figure 4 compares plots of contours of constant emissions for argon at 7 and 25 bars. The expansion of the radius $D/2$ of the waist of emission from the breakdown of 7-bar argon gas takes place at a speed of 0.7 μm ns^{-1} (see Fig. 6), which is about a factor of 2 less than the $u/2\gamma$ expansion of a neutral ideal gas with the same sound velocity. Figure 4(a) shows that the contours of constant emission for 25-bar argon steepen, if anything, and do not propagate outward. This applies in all directions. For 7 bars the plasma does not expand in the z direction, which on average is seven times longer than the waist is wide.

Regarding the lack of expansion at 25 bars, we note that one-component plasmas can demonstrate a tensile strength [25]. Whether these experiments are observing evidence for such effects will require more detailed modeling; we note that the ionization plotted in Fig. 6 should be regarded as a lower bound in view of the small deviation of emissivity from 1. Our time-resolved measurements suggest that we may be entering the regime where ion coupling and correlation effects play a significat role, which would provide a testing ground for various hydrodynamic [14,16] or kinetic [49] models that incorporate these effects.

Self-similar solutions for the expansion of a plasma into a vacuum have been derived from hydrodynamics [48,50] or kinetic [51] equations for an ideal plasma. Although our initial plasma is not surrounded by vacuum, the ambient pressure of 25 bars is small compared to the plasma pressure. For Mora [48], both the atomic density and the electron density are Gaussian. Due to the femtosecond nature of the breakdown which we study, the atomic density is best regarded as flat. However, a self-similar solution is also possible where the electron density is Gaussian and quasineutrality is maintained by a constant mass density which has a compensating space- and time-dependent ionization fraction. In this model, the electrons expand at a velocity determined by the electron and not the ion mass. Such a rapid expansion is not seen.

In general, the volume of the plasma contracts rather than expands. For an ideal gas, this contributes to heating, rather than cooling. Typical hydrodynamic equations cannot explain the macroscopic motion.

XII. CONCLUSION

Here we point to the use of Compressed Ultrafast Photography in advancing the physics of a strongly coupled

plasma for which the theory is incomplete. In this direction CUP has been used to resolve the time-dependent 2D behavior of a breakdown plasma formed from gases that are sufficiently dense that the plasma emissivity is close to unity. The key quantity measured is the plasma emission. Many physical processes contribute to the emission [52]. In order to facilitate an application of the CUP data, we have interpreted emission and absorption according to the free-free theory of plasma radiation and absorption (Bremsstrahlung and inverse Bremsstrahlung). Plasma breakdown creates an ionized medium where the mean free path of light is due to its interaction with free electrons. Although this is in many ways the simplest model, we propose that it is in fact appropriate because detailed spectral measurements [31] are smooth and lack features. Its application points to a degree of ionization that can only be explained with a reduction in the effective ionization potential that exceeds existing theories. Temperature is determined by a graybody fit and we find that an argon plasma formed at 25 bars is an isolated system for about 10 ns, during which time thermal conduction to the environment and radiative cooling are small. The two-dimensional (radial and axial) response during electron-ion equilibration is resolved. Free expansion is observed at low but not high gas density. As time progresses, ionization decreases yet we do not discern signs of recombination heating. We envision extension of this method to study 2D hydrodynamics especially during the timescales where $\Gamma > 1$. For 7-bar argon at 5.5 ns, $T = 16$ kK and $x = 2$, yielding an ion coupling coefficient $\Gamma > 3$. For these parameters the Debye screening length $\delta_D = 0.34$ nm and $\delta_D/a_0 = 0.3$ so that the ratio of Thomas-Fermi to Debye screening lengths is $\delta_{TF}/\delta_D \simeq 0.4$. Figure 1 shows just a few frames from a movie with over 250 frames of a single event with a duration of 500 ps. These systems are then testbeds for theories of equations of state and strongly coupled hydrodynamics, and sources for the unmasking of emergent properties of these systems. It appears reasonable to apply this technique to obtain a single-shot movie of processes that have been collected frame by frame using the pump-probe technique [53] and to extend its use to x-ray CUP of dynamical processes in dense systems [54].

ACKNOWLEDGMENTS

This research has been funded by the AFOSR (Grant No. FA9550-21-1-0295) and by Caltech (Carver Mead New Adventures Grant). The views, opinions, and/or findings expressed are those of the authors and should not be interpreted as representing the official views or policies of the Department of Defense or the U.S. Government. We thank T. Chuna, Z. Johnson, M. S. Murillo, and L. G. Silvestri for many valuable discussions. We are indebted to C. C. Wu for calculations of the evolution of contact discontinuities shown in Supplemental Material Fig. S13. Y.N.M. acknowledges Swedish Research Council Funding, Grant No. IPD2018-06783.

DATA AVAILABILITY

The data that support the findings of this article are not publicly available upon publication because it is not technically feasible and/or the cost of preparing, depositing, and hosting the data would be prohibitive within the terms of this research project. The data are available from the authors upon reasonable request.

[1] H. M. van Horn, Crystallization of white dwarfs, Astrophys. J. **151**, 227 (1968).
[2] H. M. van Horn, The crystallization of white dwarf stars, Nat. Astron. **3**, 129 (2019).
[3] G. E. Morfill and A. V. Ivlev, Complex plasmas: An interdisciplinary research field, Rev. Mod. Phys. **81**, 1353 (2009).
[4] T. Killian, T. Pattard, T. Pohl, and J. Rost, Ultracold neutral plasmas, Phys. Rep. **449**, 77 (2007).
[5] T. C. Killian, Ultracold neutral plasmas, Science **316**, 705 (2007).
[6] A. Bataller, A. Latshaw, J. P. Koulakis, and S. Putterman, Dynamics of strongly coupled two-component plasma via ultrafast spectroscopy, Opt. Lett. **44**, 5832 (2019).
[7] A. Bataller, G. R. Plateau, B. Kappus, and S. Putterman, Blackbody emission from laser breakdown in high-pressure gases, Phys. Rev. Lett. **113**, 075001 (2014).
[8] J. M. Maxson, Fundamental photoemission brightness limit from disorder induced heating, New J. Phys. **15**, 103024 (2013).
[9] S. Atzeni and J. Meyer-Ter-Vehn, *The Physics of Inertial Fusion: Beam Plasma Interaction, Hydrodynamics, Hot Dense Matter, International Series of Monographs on Physics* (Clarendon Press, Oxford, UK, 2004).
[10] D. Saumon, C. Starrett, J. Anta, W. Daughton, and G. Chabrier, The structure of warm dense matter modeled with an average atom model with ion-ion correlations, in *Frontiers and Challenges in Warm Dense Matter*, edited by F. Graziani, M. P. Desjarlais, R. Redmer, and S. B. Trickey (Springer, New York, 2014), pp. 151–176.
[11] L. Gao, J. Liang, C. Li, and L. V. Wang, Single-shot compressed ultrafast photography at one hundred billion frames per second, Nature (London) **516**, 74 (2014).
[12] P. Wang and L. V. Wang, Compressed ultrafast photography, in *Coded Optical Imaging*, edited by J. Liang (Springer International Publishing, Cham, 2024), pp. 453–480.
[13] J. P. Hansen, Statistical mechanics of dense ionized matter. I. Equilibrium properties of the classical one-component plasma, Phys. Rev. A **8**, 3096 (1973).
[14] A. Diaw and M. S. Murillo, Generalized hydrodynamics model for strongly coupled plasmas, Phys. Rev. E **92**, 013107 (2015).
[15] M. D. Acciarri, C. Moore, and S. D. Baalrud, Strong coulomb coupling influences ion and neutral temperatures in atmospheric pressure plasmas, Plasma Sources Sci. Technol. **31**, 125005 (2022).
[16] D. Krimans and S. Putterman, Variational principles for the hydrodynamics of the classical one-component plasma, Phys. Fluids **36**, 037131 (2024).
[17] See Supplemental Material at http://link.aps.org/supplemental/10.1103/3vw9-h2g5 for 4 example CUP-reconstructed videos

of single plasma events; more detailed descriptions of the experimental setup, and the CUP image formation, characterization, and calibration process; and simulations of the evolution of a 1D contact discontinuity in an ideal gas.

[18] G. Dimonte and J. Daligault, Molecular-dynamics simulations of electron-ion temperature relaxation in a classical coulomb plasma, Phys. Rev. Lett. **101**, 135001 (2008).

[19] R. R. Goforth and P. Hammerling, Recombination in an expanding laser-produced plasma, J. Appl. Phys. **47**, 3918 (1976).

[20] A. M. Abd El-Hameed, I. Azzouz, G. Abou-Koura, and Y. E.-D. Gamal, Study of recombination processes during the expansion phase of titanium-plasma produced by picosecond nd:Glass laser radiation, Nucl. Instrum. Methods Phys. Res., Sect. B **205**, 271 (2003).

[21] B. Kappus, A. Bataller, and S. J. Putterman, Energy balance for a sonoluminescence bubble yields a measure of ionization potential lowering, Phys. Rev. Lett. **111**, 234301 (2013).

[22] A. Bataller, S. Putterman, S. Pree, and J. Koulakis, Observation of shell structure, electronic screening, and energetic limiting in sparks, Phys. Rev. Lett. **117**, 085001 (2016).

[23] J. C. Stewart and K. D. Pyatt, Jr., Lowering of ionization potentials in plasmas, Astrophys. J. **144**, 1203 (1966).

[24] B. Crowley, Continuum lowering – a new perspective, High Energy Density Phys. **13**, 84 (2014).

[25] S. G. Brush, H. L. Sahlin, and E. Teller, Monte carlo study of a one-component plasma. I, J. Chem. Phys. **45**, 2102 (1966).

[26] G. R. Arce, D. J. Brady, L. Carin, H. Arguello, and D. S. Kittle, Compressive coded aperture spectral imaging: An introduction, IEEE Signal Process. Mag. **31**, 105 (2014).

[27] P. Llull, X. Liao, X. Yuan, J. Yang, D. Kittle, L. Carin, G. Sapiro, and D. J. Brady, Coded aperture compressive temporal imaging, Opt. Express **21**, 10526 (2013).

[28] K. Choi and D. J. Brady, Coded aperture computed tomography, in *Adaptive Coded Aperture Imaging, Non-Imaging, and Unconventional Imaging Sensor Systems*, edited by D. P. Casasent, S. Rogers, J. J. Dolne, T. J. Karr, and V. L. Gamiz (International Society for Optics and Photonics, SPIE, Bellingham, WA, 2009), Vol. 7468, p. 74680B.

[29] D. Qi, S. Zhang, C. Yang, Y. He, F. Cao, J. Yao, P. Ding, L. Gao, T. Jia, J. Liang, Z. Sun, and L. V. Wang, Single-shot compressed ultrafast photography: A review, Adv. Photonics **2**, 014003 (2020).

[30] K. Adzerikho and V. Nekrasov, Luminescence characteristics of cylindrical and spherical light-scattering media, Int. J. Heat Mass Transf. **18**, 1131 (1975).

[31] A. W. Bataller, Exploring the universality of sonoluminescence, Ph.D. thesis, University of California, Los Angeles, 2014.

[32] A. Bataller, B. Kappus, C. Camara, and S. Putterman, Collision time measurements in a sonoluminescing microplasma with a large plasma parameter, Phys. Rev. Lett. **113**, 024301 (2014).

[33] S. D. Baalrud and J. Daligault, Effective potential theory for transport coefficients across coupling regimes, Phys. Rev. Lett. **110**, 235001 (2013).

[34] Y. B. Zel'dovich and Y. P. Raizer, in *Physics of Shock Waves and High-Temperature Hydrodynamic Phenomena* (Dover, Mineola, NY, 2002), p. 259.

[35] J. P. Kinney, H. J. LeFevre, C. C. Kuranz, and S. D. Baalrud, Mean force emission theory for classical bremsstrahlung in strongly coupled plasmas, Phys. Plasmas **31**, 053302 (2024).

[36] Y. B. Zel'dovich and Y. P. Raizer, in *Physics of Shock Waves and High-Temperature Hydrodynamic Phenomena* (Dover, Mineola, NY, 2002), pp. 115–118.

[37] L. D. Landau and E. M. Lifshitz, *Fluid Mechanics Second Edition* (Elsevier, Burlington, MA, 1987), p. 207.

[38] Y. B. Zel'dovich and Y. P. Raizer, in *Physics of Shock Waves and High-Temperature Hydrodynamic Phenomena* (Dover, Mineola, NY, 2002), p. 417.

[39] L. G. Stanton and M. S. Murillo, Ionic transport in high-energy-density matter, Phys. Rev. E **93**, 043203 (2016).

[40] Y. K. Kurilenkov and A. A. Valuev, The electrical conductivity of plasma in wide range of charge densities, Contrib. Plasma Phys. **24**, 161 (1984).

[41] J. Ferch, B. Granitza, C. Masche, and W. Raith, Electron-argon total cross section measurements at low energies by time-of-flight spectroscopy, J. Phys. B **18**, 967 (1985).

[42] Y. B. Zel'dovich and Y. P. Raizer, in *Physics of Shock Waves and High-Temperature Hydrodynamic Phenomena* (Dover, Mineola, NY, 2002), pp. 518–519.

[43] M. S. Murillo, Using fermi statistics to create strongly coupled ion plasmas in atom traps, Phys. Rev. Lett. **87**, 115003 (2001).

[44] B. Kappus, S. Khalid, A. Chakravarty, and S. Putterman, Phase transition to an opaque plasma in a sonoluminescing bubble, Phys. Rev. Lett. **106**, 234302 (2011).

[45] S. Lee, J. Lee, Y. D. Yoon, D. E. Kim, and G. Yun, Characterization of strongly coupled plasmas produced in argon supercritical fluids, Plasma Phys. Controlled Fusion **64**, 095010 (2022).

[46] D. Turnbull, J. Katz, M. Sherlock, L. Divol, N. R. Shaffer, D. J. Strozzi, A. Colaïtis, D. H. Edgell, R. K. Follett, K. R. McMillen, P. Michel, A. L. Milder, and D. H. Froula, Inverse bremsstrahlung absorption, Phys. Rev. Lett. **130**, 145103 (2023).

[47] T. V. Tsankov, R. Johnsen, and U. Czarnetzki, Rydberg state, metastable, and electron dynamics in the low-pressure argon afterglow, Plasma Sources Sci. Technol. **24**, 065001 (2015).

[48] P. Mora, Collisionless expansion of a gaussian plasma into a vacuum, Phys. Plasmas **12**, 112102 (2005).

[49] T. Pohl, T. Pattard, and J. M. Rost, Kinetic modeling and molecular dynamics simulation of ultracold neutral plasmas including ionic correlations, Phys. Rev. A **70**, 033416 (2004).

[50] M. Murakami, Y.-G. Kang, K. Nishihara, S. Fujioka, and H. Nishimura, Ion energy spectrum of expanding laser-plasma with limited mass, Phys. Plasmas **12**, 062706 (2005),.

[51] D. S. Dorozhkina and V. E. Semenov, Exact solution of vlasov equations for quasineutral expansion of plasma bunch into vacuum, Phys. Rev. Lett. **81**, 2691 (1998).

[52] *Modern Methods in Collisional-Radiative Modeling of Plasmas*, edited by Y. Ralchenko (Springer International Publishing, Cham, 2016).

[53] X. Gao, G. Patwardhan, S. Schrauth, D. Zhu, T. Popmintchev, H. C. Kapteyn, M. M. Murnane, D. A. Romanov, R. J. Levis, and A. L. Gaeta, Picosecond ionization dynamics in femtosecond filaments at high pressures, Phys. Rev. A **95**, 013412 (2017).

[54] H. Zhou, Z. Yao, L. Sheng, Y. Song, Z. Liu, C. Han, Z. Zhu, Y. Li, B. Duan, C. Ji, J. Wu, D. Hei, and Y. Liu, X-ray compressed ultrafast photography under the constraint of time-integrated-image for x-pinch, Optics Lasers Eng. **183**, 108508 (2024).